Journal of Materials Chemistry A

Accepted Manuscript

This article can be cited before page numbers have been issued, to do this please use: Y. Zhu, C. Cao, W. Jiang, S. Yang, J. Hu, W. Song and L. Wan, *J. Mater. Chem. A*, 2016, DOI: 10.1039/C6TA08335H.

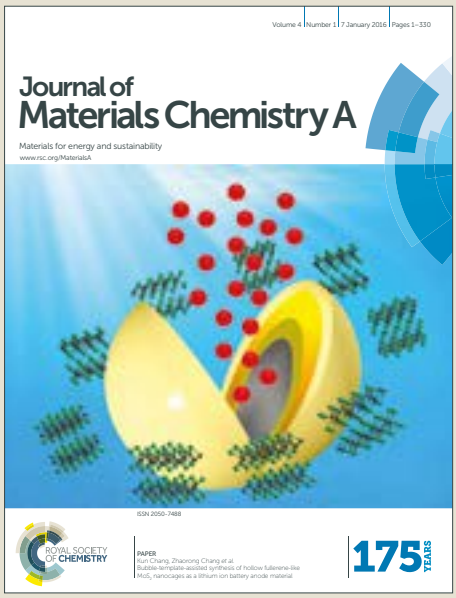

This is an Accepted Manuscript, which has been through the Royal Society of Chemistry peer review process and has been accepted for publication.

Accepted Manuscripts are published online shortly after acceptance, before technical editing, formatting and proof reading. Using this free service, authors can make their results available to the community, in citable form, before we publish the edited article. We will replace this Accepted Manuscript with the edited and formatted Advance Article as soon as it is available.

You can find more information about Accepted Manuscripts in the author guidelines.

Please note that technical editing may introduce minor changes to the text and/or graphics, which may alter content. The journal's standard Terms & Conditions and the ethical guidelines, outlined in our author and reviewer resource centre, still apply. In no event shall the Royal Society of Chemistry be held responsible for any errors or omissions in this Accepted Manuscript or any consequences arising from the use of any information it contains.

ROYAL SOCIETY OF CHEMISTRY

rsc.li/materials-a

View Article Online
DOI: 10.1039/C6TA08335H

Journal Name

ARTICLE

Nitrogen, Phosphorus and Sulfur co-doped Ultrathin Carbon Nanosheet as a Metal-free Catalyst for Selective Oxidation of Aromatic Alkanes and Oxygen Reduction Reaction

Received 00th January 20xx,
Accepted 00th January 20xx

DOI: 10.1039/x0xx00000x

www.rsc.org/

Ya-Nan Zhu,[ab] Chang-Yan Cao,*[ab] Wen-Jie Jiang,[ab] Shu-Liang Yang,[ab] Jin-Song Hu,[a] Wei-Guo Song*[ab] and Li-Jun Wan*[a]

Carbon materials have attracted considerable interests as metal-free heterogeneous catalysts owing to their superior physiochemical properties, including low-cost, stability, easily tailorable structures as well as excellent catalytic activity. In this study, we have designed an efficient method to produce ultrathin carbon nanosheets (~ 2.2 nm) with multi-heteroatom (nitrogen, phosphorus and sulfur) doping and high surface area (up to 1198 m^2 g^{-1}). This method employs poly(cyclotriphosphazene-co-4,4'-sulfonyldiphen-ol) (PZS) as main carbon source and N, P, S-doping sources, while g-C_3N_4 nanosheets act as morphology templates, extra N doping source and porogen. The doped carbon nanosheet is an excellent metal-free carbocatalyst for selective oxidation of aromatic alkanes in aqueous solution and electrochemical catalyst for oxygen reduction reaction in alkaline medium.

1.Introduction

Carbon materials, including active carbon, carbon nanotubes, graphene, carbon dot, carbon nanodiamond, fullerenes, etc., have shown promising applications in adsorption,[1-5] batteries,[5-9] supercapacitors[10-13] and catalysis[14-17]. Particularly, the unique physicochemical properties of carbon materials, including excellent stability in both acidic and basic media, easily tailorable structures and surface functionizations, are very beneficial for catalysis.[13] In recent years, rapid progress has been achieved in the development of various carbon-based materials as low-cost and benign heterogeneous catalysts for organic reactions and electrocatalysts for oxygen reduction and hydrogen evolution reactions (ORR-HER)[18-22]. A facile and controllable method to synthesize carbon material with desirable morphology and structure, as well as superior catalytic performance is always pursued in this field.

The local structure played an important role in the catalytic behaviors of carbon catalysts.[22] Optimizing the structure of carbon materials can result in high surface area and pore volume, which will increase the number of accessible reactive sites and accelerate the mass transport.[13] Studies have also shown that heteroatom doping (N, P, S, B, etc.) was critical to change the electronic structure of adjacent carbon and/or produce additional active sites, thus improving the catalytic performance of carbon materials.[18-21,23] Specially, doping carbon with two or more selected heteroatoms will further improve the catalytic activity because of the synergistic effects between heteroatoms.[21,24-27] Comparing to single dopant, multi-dopants will introduce larger asymmetrical spin and charge density on active carbon atoms. However, directly adding external molecules containing multi-heteroatoms into the carbon source is hard. It's difficult to control the structures and dopants status of carbon catalysts. Therefore, it is desired to find a rational way to obtain carbon materials with controlled multi-dopants as well as controlled structure with porous and high surface area.

Pyrolyzing a precursor containing heteroatoms enables the preparation of carbon materials with multi-dopants at molecular-level, and casting with hard or soft templates enables controlled mesoscopic morphology and microstructure.[28] In previous work, we developed a facile method to produce nitrogen, phosphorus, and sulfur co-doped hollow carbon shells using poly(cyclo-triphosphazene-co-4,4'-sulfonyldiphenol) (denoted as PZS) as carbon and heteroatoms source, and metal-organic framework (MOF) ZIF-67 as structure template.[29] However, Co_2P nanoparticles were formed during the calcination process, requiring acid-etching to obtain the final metal-free hollow carbon shells.

In this study, we found a better method to prepare nitrogen, phosphorus, and sulfur atoms co-doped carbon nanosheets (denoted as NPS-CNS) using g-C_3N_4 nanosheets template. The procedure for preparing NPS-CNS is illustrated in Scheme 1. g-C_3N_4 nanosheets were first prepared via thermal decomposition of urea[30]. Subsequently, highly cross-linked PZS was coated on the both sides

[a] Beijing National Laboratory for Molecular Sciences, Laboratory of Molecular Nanostructures and Nanotechnology, Institute of Chemistry, Chinese Academy of Sciences, Beijing, 100190, P.R. China. E-mail: E-mail: cycao@iccas.ac.cn; wsong@iccas.ac.cn; wanlijun@iccas.ac.cn
[b] University of Chinese Academy of Sciences, Beijing, 100049, P.R. China.

Electronic Supplementary Information (ESI) available: TEM images of controlled samples, Raman spectra and XRD patterns of NPS-CNS-300-Y, TG curve of g-C_3N_4, XPS analysis, reusability of NPS-CNS-300-1000 for ethylbenzene oxidation. See DOI: 10.1039/x0xx00000x

View Article Online
DOI: 10.1039/C6TA08335H

of g-C_3N_4 nanosheets. Finally, g-C_3N_4@PZS nanosheets were calcined at desired temperature in Ar atmosphere, resulting in pyrolysis of g-C_3N_4 nanosheets and simultaneously carbonization of PZS layer. During this calcination process, nitrogen, phosphorus, and sulfur atoms in the PZS were uniformly doped into the carbon nanosheets. At the same time, g-C_3N_4 decomposed completely and led to three beneficial results: no post process was needed to remove the template; mesoporosity and surface area was enhanced; total doping amount of nitrogen atom was increased. All these features make the synthesis route a highly efficient way to fabricate multi-heteroatoms co-doped carbon nanosheets with high surface area. The prepared NPS-CNS can be used as a metal-free heterogeneous catalyst with excellent properties for selective oxidation of aromatic alkanes in aqueous solution and electrochemical catalyst for oxygen reduction reaction in alkaline medium.

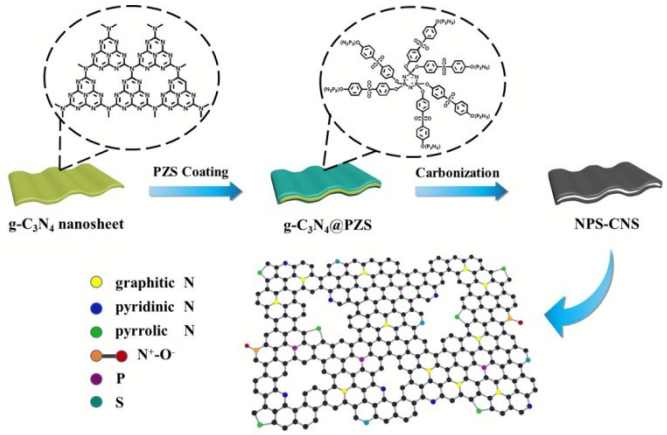

Scheme 1. Schematic illustration for preparing nitrogen, phosphorus and sulfur co-doped ultrathin carbon nanosheet.

2. Experimental section

2.1 Materials

Urea (A.R.) was purchased from Beijing Chemical Reagent Company. Ethylbenzene (99%), anisole (99%), 4-ethylanisole (98+%), cumene (99%), diphenylmethane (99+%), fluorene (98+%), tertbutyl hydroperoxide (70% aqueous solution), hexachlorocyclo-phosphazene (98%) and 4,4'-sulfonyldiphenol (99%) were provided by Alfa-Aesar. 2-ethylnaphthalene (99%) was purchased from TCI. 1-ethyl-4-nitrobenzene (98+%) was purchased from Adamas. Triethylamine (99%) was purchased from J&K scientific Co., Ltd.

2.2 Catalyst preparation

***Synthesis of g-C_3N_4 nanosheets*:** g-C_3N_4 nanosheets were produced according to a procedure described in a previous paper. In a typical experiment, 10 g of urea was placed in a crucible with a cover, and then it was heated at 550°C in a muffle furnace for 2h. The resulted yellow powder was collected for use without further treatment.

Synthesis of doped carbon nanosheets(NPS-CNS): A certain amount of g-C_3N_4 powders were dispersed into 160 mL methanol under ultrasound. Then another solution containing 280 mg of hexachlorocyclophosphazene and 630 mg of 4, 4'-sulfonyldiphenol in 26 mL of methanol was added drop by drop. After stirring for five minutes, 0.74mL of triethylamine was added dropwise and the solution was continued to stir for 6 h. Then, the yellow precipitates were collected and washed with methanol for three times and dried under vacuum at room temperature for overnight. The above obtained g-C_3N_4@PZS products were calcined at desired temperature for 2 h in a tubular furnace under argon atmosphere.

2.3 Catalyst Characterizations

X-ray diffraction (XRD) patterns were performed on a Rigaku D/max-2500 diffractometer with Cu Kα radiation (λ= 1.5418 Å) at 40 kV and 200 mA. The microstructures of the samples were characterized by high-resolution transmission electron microscopy (JEOL, JEM-2100F). XPS measurement was performed on the VG Scientific ESCALab220i-XL spectrometer using Al Kα radiation. The surface area of the products was measured by the Brunauer–Emmett–Teller (BET) method using N_2 adsorption and desorption isotherms on an Autosorb-1 analyzer at 77 K.

2.4 Catalytic activity test

Oxidation of aromatic alkanes catalytic test: Substrate (0.5 mmol), catalyst (8.0 mg), TBHP (500 µL, 70 wt% in water), and water (1 mL) were added into a 15 mL glass reaction tube sealed with a Teflon lid. The reaction mixture was stirred in a preheated 80 ºC oil bath for 12 h. Then 77 µL anisole was added to the system as internal standard. 10 mL CH_2Cl_2 was added to extract organic compounds in the reaction system. The organic phase was analyzed by GC (Shimadzu GC-2010) equipped with a flame ionization detector (FID) and a Rtx-5 capillary column (0.25 mm in diameter, 30 m in length). The identity was ascertained by GC-MS (Shimadzu GCMS-QP2010S) with a HP-5MS capillary column (0.25 mm in diameter, 30 m in length). In recycle experiments, reaction time was shortened from 12 h to 6 h, and the catalyst was separated by centrifugation and washed with ethanol three times and dried under vacuum at 60 ºC for 6 h. The recovered catalyst was reused in the next run.

Electrocatalytic oxygen reduction reaction test: Prior to test, the rotating ring-disk electrode (RRDE, 4 mm in diameter for disk) was polished mechanically with alumina slurry to get a mirror-like surface and then washed with ethanol and allowed to dry. In a typical procedure for ink preparation, 5 mg catalysts were dispersed in 1 mL ethanol and sonicated for 30 min to form a homogeneous ink. Then, 15 uL ink was loaded on polished RRDE to produce a catalyst loading of 0.6 mg cm^{-2}. A drop of 0.5 wt% Nafion (Sigma-Aldrich) solution was then applied onto electrode surface layer to protect the catalyst from dropping out. After drying in air, the electrode was ready for tests. Commercially available Johnson-Matthey Pt/C with 20 wt% Pt loading was used for comparison. The loading of Pt/C catalyst was 0.127 mg cm_{Pt+C}^{-2}. Electrocatalytic measurements were carried out on a RRDE-3A (ALS, Japan) device in conjunction with an electrochemical workstation Autolab PGSTAT 302N (Metrohm, The Netherlans). The cell consisted of a RRDE with a glassy carbon disk of 4 mm in diameter as working electrode, an Ag/AgCl (saturated KCl) as reference electrode (BASi) and a Pt wire as counter electrode. Before each ORR test, the electrolyte was purged with O_2 for at least 30 min. All the LSV measurements were conducted at a rotation speed of 1600 rpm. The potential on the ring electrode for each RRDE tests was set to 1.5 V (vs. RHE), which

View Article Online
DOI: 10.1039/C6TA08375H

is high enough for oxidizing the peroxide species produced from disk electrode. The electron transfer number (n) was calculated using the following equation:

$$n = 4 \times \frac{j_d}{j_d + j_r / N}$$

while j_d and j_r are the current densities on disk and ring electrodes, respectively. N is the ring collection efficiency and the measured N value was 42.4%.

3. Results and discussion

Samples with different contents of g-C_3N_4 and calcined at different temperatures were labeled as NPS-CNS-X-Y, X represents the amount of g-C_3N_4 (mg) and Y represents the calcination temperature (°C). Typical transmission electron microscopy (TEM) images of the samples in each step during preparation of NPS-CNS-300-1000 were shown as an example. g-C_3N_4 nanosheets were successfully prepared by thermal decomposition of urea (Fig. S1a†). After coating PZS, g-C_3N_4@PZS retained nanosheet structures (Fig. S1b). For comparison, only solid spheres of PZS were formed in the absence of g-C_3N_4 (Fig. S2), indicating g-C_3N_4 nanosheets played an important role in acting as hard template for PZS coating. The final NPS-CNS-300-1000 showed sheet-like structure (Fig. 1a), suggesting the ultrathin feature of nanosheets. Representative atomic force microscope (AFM) images indicated that the thickness of nanosheets was around 4.4 nm. Because PZS were coated on the both sides, the NPS-CNS nanosheets were actually composed of two layers with a very thin void space in between. Thus, the average thickness of NPS-CNS-300-1000 layer was only about 2.2 nm (Fig. 1b). High-resolution TEM image (Fig. 1c) showed the obvious interlayer distance of 0.34 nm corresponding to the (002) plane of graphite, revealing the graphitic nature of doped carbon nanosheets. Raman spectrum of NPS-CNS-300-1000 (Fig. S3) showed two peaks at 1350 and 1590 nm, assigned to disordered sp^3 carbon (D band) and graphitic sp^2 carbon (G band), respectively.[31,32] The I_D/I_G intensity ratio was 0.95, further confirming the graphitic structure. Fig. S4 showed the powder X-ray diffraction (XRD) pattern of NPS-CNS-300-1000. It can be seen that a broad peak at 24°, corresponding to (002) planes of graphite. No peak of g-C_3N_4 was observed, suggesting the complete decomposition of g-C_3N_4 during the 1000 °C treatment. Thermogravimetric analysis (TGA) confirmed that g-C_3N_4 nanosheet can be total decomposed below 680 °C (Fig. S5).

Energy dispersive spectroscopy (EDS) mapping of NPS-CNS-300-1000 using scanning transmission electron microscopy (STEM) (Fig. 1d) revealed that homogeneous distribution of nitrogen, phosphorus, and sulfur atoms throughout the carbon nanosheets, indicating that these heteroatoms were simultaneously doped during thermal calcination. Such multi-heteroatoms doping with high dispersion through one step annealing was better compare to traditional doping methods.[33-36]

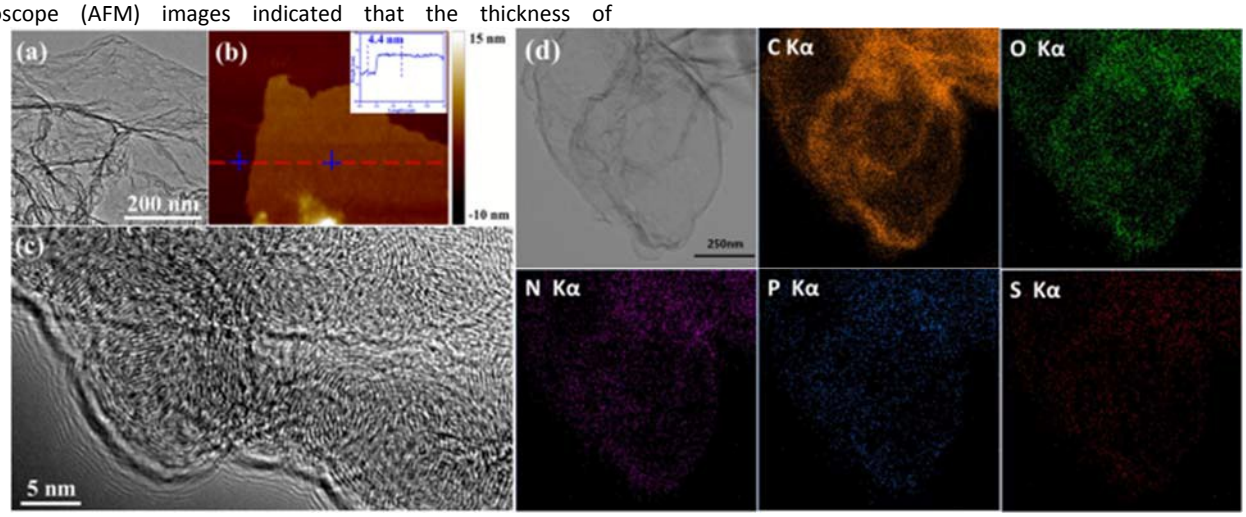

Fig.1 TEM images of (a) TEM, (b) AFM and (c) HRTEM images of NPS-CNS-300-1000, (d) EDS mapping of NPS-CNS-300-1000.

In order to characterize the nitrogen, phosphorus, and sulfur dopants in the carbon nanosheet, X-ray photoelectron spectroscopy (XPS) analysis was performed. As shown in Fig. 2a and Table S1, the XPS survey spectrum confirmed that NPS-CNS-300-1000 was N, P and S co-doped with the contents of 2.32 at%, 0.68 at% and 0.49 at%, respectively. For comparison, the contents of N, P and S in pure PZS nanospheres after being calcined at 1000 °C (denoted as PZS-1000) were 1.18 at%, 0.74 at% and 0.7 at%, respectively. Note that the N ratio in NPS-CNS-300-1000 was nearly two times higher than that in calcined pure PZS nanospheres, suggesting some N atoms in g-C_3N_4 were also doped into the carbon nanosheets during calcination. These results showed that g-C_3N_4 nanosheet could also act as extra N doping source, enhancing the total amount of N in the NPS-CNS. The high-resolution N1s spectrum of NPS-CNS-300-1000 was shown in Fig. 2b. It can be divided into three peaks at 398.3 eV (pyridinic N), 401.1 eV (graphitic N) and 403.5 eV (pyridinic N^+-O^-) with ratios of 16.9 %, 70.0 % and 13.1 %, respectively (Fig. S7a).[29,37] The high-resolution P2p spectrum displayed two peaks at approximately 132.5 eV and 133.7 eV, corresponding to P-C and P-O, respectively (Fig. 2c). The S2p spectrum fit well with three peaks at 163.8, 165.1, and 168.2 eV, which were ascribed to $2p^{3/2}$, $2p^{1/2}$ splitting of the S2p spin orbital (-C-S-C-) and oxidized S, respectively (Fig. 2d).

View Article Online
DOI: 10.1039/C6TA08735H

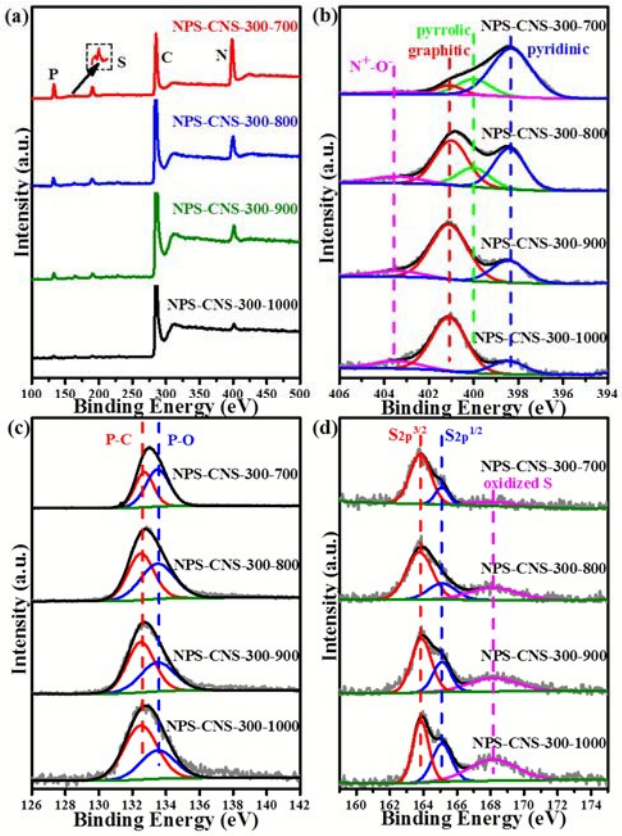

Fig.2 XPS spectra of NPS-CNS-300-Y: (a) survey, (b) N1s, (c) P2p, and (d) S2p.

The structure, species of dopants and the special surface area of carbon nanosheets can be easily controlled by the carbonization temperature. For example, samples of NPS-CNS-300 after calcined at 700 °C, 800 °C and 900 °C were prepared and investigated by TEM, XRD, Raman and XPS. All products showed nanosheet structures without obvious difference (Fig. S6). XRD patterns revealed the intensity of graphite peak at 24° decreased gradually from NPS-CNS-300-1000 to NPS-CNS-300-700 (Fig. S4). No diffraction peaks of g-C_3N_4 were observed in all samples, further confirming the complete decomposition of g-C_3N_4 nanosheet above 680 °C. Raman spectra also showed the slightly decreasement of I_D/I_G values (Fig. S3), indicating the improvement of graphitization degree with the elevated calcination temperature, which was agreed with XRD result. As shown in Fig. 2a, N, P and S signals were also observed in the XPS survey of all samples. The atomic ratios were summarized in Table S1. It can be seen that the carbon content increased while the oxygen, nitrogen and phosphorus contents decreased with increasing carbonization temperature. Sulfur content was also increased under higher temperature. N1s spectra showed that the species of nitrogen were obviously different, and graphitic N became dominant with increasing calcination temperature. The relative ratio of graphitic N in NPS-CNS-300-1000 was the highest (Fig. 2b and Fig. S7a). P2p spectra for all samples showed the ratio of P-C increased while ratio of P-O decreased under higher temperature (Fig. 2c and Fig. S7b). S2p spectra showed the increasement ratio of oxidized S species (Fig. 2d and Fig. S7c), suggesting sulfur and oxygen atoms were more likely to combine under higher calcination temperature to form stable sulfate. This may explain the increasement of sulfur content under elevating calcination temperatures.

The N_2 adsorption-desorption isotherms of all NPS-CNS-300-Y samples showed a typical-IV curve (Fig. 3a), indicating the existence of both micro- and mesopores. The BET specific surface areas of NPS-CNS-300-700, NPS-CNS-300-800, NPS-CNS-300-900 and NPS-CNS-300-1000 were 330, 755, 807 and 1198 $m^2\ g^{-1}$, respectively. For comparison, the N_2 adsorption-desorption isotherms of PZS-1000 obtained without g-C_3N_4 nanosheet template showed a typical type I curve, suggesting only microporosity. The BET specific surface area was only about 562 $m^2\ g^{-1}$ for PZS-1000. The released gases during the thermal decomposition of g-C_3N_4 nanosheets introduce additional mesopores, and thus enhance the surface area of carbon nanosheets. Based on the results above, the highest surface area of NPS-CNS-300-1000 likely relate to the highly carbonization degree, ultrathin nanosheet structure and numerous pores.

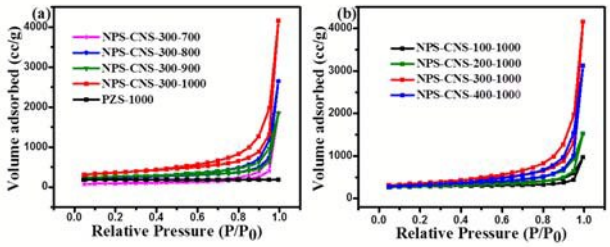

Fig.3 N_2 adsorption-desorption isotherms of (a) PZS-1000 and NPS-CNS-300-Y, (b) NPS-CNS-X-1000.

Furthermore, the structure, the amount of dopants and the special surface area of carbon nanosheets can also be controlled by the ratio of g-C_3N_4 nanosheet template to PZS layer. For example, products of NPS-CNS-100-1000, NPS-CNS-200-1000 and NPS-CNS-400-1000 were also prepared. All the samples showed nanosheet-like structures (Fig. S8), similar to that of NPS-CNS-300-1000. No serious aggregation was observed, indicating the homogeneous coating of PZS layer in all samples. Carbon nanosheets were expected to be thinner when more g-C_3N_4 templates were added. However, due to the stacking and wrinkles of nanosheets, it was hard to accurately measure the thickness difference of carbon nanosheets. The BET special surface area of NPS-CNS-100-1000, NPS-CNS-200-1000 and NPS-CNS-400-1000 were 873, 915 and 1031 $m^2\ g^{-1}$, respectively (Fig. 3b and Table S1). NPS-CNS-300-1000 had the highest surface area of 1198 $m^2\ g^{-1}$. XPS survey results showed a slightly increasement of N dopant amount from 1.7 at% to 2.48 at% for NPS-CNS-100-1000 to NPS-CNS-400-1000. This result further confirmed that some N atoms in g-C_3N_4 were doped into the carbon nanosheets during calcination. There was no obvious difference of N1s, P2p and S2p spectra in these samples (Fig. S9).

Based on the above results, we can conclude that g-C_3N_4 nanosheet template played very important roles in the formation of final NPS-CNS. First, g-C_3N_4 nanosheet was the structural template for coating of PZS layer, which was subsequently calcined to form the nanosheet. Second, the complete decomposition of g-C_3N_4 nanosheets above 680 °C made the synthesis route convenient. Third, some N atoms in g-C_3N_4 were also doped into the carbon

nanosheets during calcination, increasing the total amount of N doping in the final NPS-CNS. Finally, the released gases during the decomposition of g-C_3N_4 nanosheets helped to introduce additional mesoporosity and to improve the specific surface area of carbon nanosheets.

The multi-heteroatom dopants, high surface area and ultrathin nanosheet structure of the obtained carbon nanosheets were expected to be very beneficial for metal-free heterogeneous catalysis. The selective oxidation of aromatic alkanes is one of the most important C-H activation reactions in organic synthesis. [38-41] Generally, noble or transition metal based catalysts are used.[41-44] However, the cost and contamination issues of these catalysts make it appealing for carbocatalyst.[29,37,45-47] Apparently, the activity of a carbocatalyst is associated with its structure, especially the specific surface area and dopants. The selective oxidation of aromatic alkanes was thus chosen to evaluate the catalytic ability of the prepared NPS-CNS.

Ethylbenzene was first chosen as the model substrate to explore the efficiency of the prepared NPS-CNS. The catalytic performances of various catalysts were listed in Table 1. About 12.4% conversion of ethylbenzene and 58.0% selectivity to acetophenone in 6 h were observed in the absence of catalyst (Table 1, entry 1). With PZS-1000, the conversion of ethylbenzene increased to 20.5% with a acetophenone selectivity of 62.3% (Table 1, entry 2). 83.5% conversion and 96.4% selectivity to acetophenone in 6 h was achieved with NPS-CNS-300-1000 catalyst (Table 1, entry 6). Obviously, NPS-CNS-300-1000 showed the best performance than other NPS-CNS catalysts (Table 1, entries 3-5, 7-9) and much better than nitrogen-doped graphene reported in the literature under similar conditions.[12] Furthermore, 96.1% conversion with acetophenone selectivity of 99.1% was obtained when the reaction time was prolonged to 12 h (Table 1, entry 11).

Table 1. Catalytic properties of different carbon catalysts for ethylbenzene selective oxidation

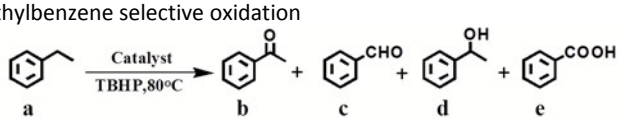

a b c d e

Entry	Catalyst	Time	Conv (%)	Sel (%)			
				b	c	d	e
1	——	6h	12.4	58.0	21.2	6.5	14.3
2	PZS-1000	6h	20.5	62.3	16.3	5.3	16.1
3	NPS-CNS-300-700	6h	14.8	62.3	16.3	5.3	16.1
4	NPS-CNS-300-800	6h	60.4	78.5	7.4	2.3	11.8
5	NPS-CNS-300-900	6h	70.8	84.1	9.7	2.9	3.3
6	NPS-CNS-300-1000	6h	83.5	96.4	2.3	1.2	0.1
7	NPS-CNS-100-1000	6h	57.2	78.5	7.4	2.3	11.8
8	NPS-CNS-200-1000	6h	77.5	97.0	1.2	1.8	0
9	NPS-CNS-400-1000	6h	78.7	95.5	2.9	1.2	0.4
10[f]	NPS-CNS-300-1000	6h	91.6	96.1	0.8	0.8	0
11[f]	NPS-CNS-300-1000	12h	96.1	99.1	0.5	0.4	0

Reaction conditions: catalyst (5 mg), TBHP (0.5 mL,70 wt% in water), substrate (0.5 mmol), H_2O (1.0 mL), 80 ºC. [f] Catalyst: 8 mg

The superior activity of NPS-CNS-300-1000 can be ascribed to the synergistic effect between the high surface area and the multi-heteroatom dopants in the carbon nanosheets. Specific surface area influences the mass transportation, while dopants change the electronic structure of carbon and/or create active sites. Ma et al. investigated the mechanism of N-doped graphene for oxidation of C-H bond in detail and suggested that graphitic N was pivotal for the C-H bond activation, as N doping atoms changed the electronic structure of the adjacent carbon atoms and promoted the catalytic reactivity.[37] NPS-CNS-300-1000 possessed the highest ratio of graphite N (Fig. S7a). NPS-CNS-300-1000 also had the highest specific surface area. It is still unclear how does phosphorus and sulfur dopants affect the catalytic property, many literatures reported their abilities in modulating the electronic structure of carbon atoms.[48-54] All these features render NPS-CNS-300-1000 a superior active metal-free catalyst for selective oxidation of aromatic alkanes. Various benzyl aromatic alkanes could be oxidized with high yields with NPS-CNS-300-1000 catalyst (Table 2). Besides the excellent activity, NPS-CNS-300-1000 also showed good stability (Fig. S10).

Table 2 Oxidation property of NPS-CNS-300-1000 catalyst for other aromatic alkanes

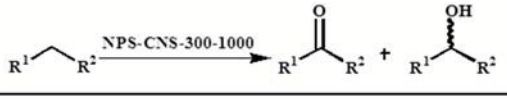

Entry	Substrate	Product	Conv (%)	Sel (%)
1			96	99
2	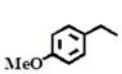	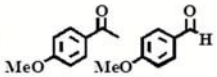	84	5.22:1
3	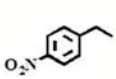	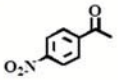	92	99
4	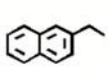	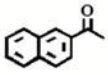	>99	>99
5		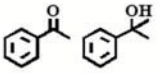	84	1:3.4
6	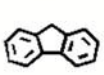	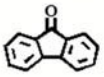	>99	>99
7	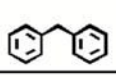	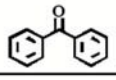	>99	>99

Reaction conditions: catalyst (8 mg), TBHP (0.5 mL, 70 wt% in water), substrate (0.5 mmol), H_2O (1.0 mL), 80 ºC, 12 h.

Electrocatalytic oxygen reduction reaction (ORR) plays a key role in fuel cells and metal–air batteries.[55] Although platinum-based electrocatalysts have been very effective for ORR, the high cost and low natural abundance of Pt propel research for noble-free alternatives.[56-58] In recent years, carbon-based materials have shown potential as ORR electrocatalysts.[23,26,59-61] The features of NPS-CNS, such as multi-heteroatom dopants, high surface area, are very beneficial for ORR.

The electrocatalytic activity of NPS-CNS-300-1000 as ORR catalysts was first studied through cyclic voltammetry (CV). As

DOI: 10.1039/C6TA08335H

shown in Fig. 4a, no obvious oxidation or reduction peak was observed under N_2 atmosphere. In comparison, a large oxygen reduction peak appeared in O_2-saturated KOH solution (0.1 M), indicating NPS-CNS-300-1000 possessed oxygen reduction activity with a high onset potential of 0.938 V. The electrocatalytic performance was further evaluated with the linear scan voltammogram (LSV). As shown in Fig. 4b, the NPS-CNS-300-1000 exhibited a half-potential of 0.800 V, which is only about 50 mV lower than that of commercial Pt/C catalyst (Johnson-Matthey). Besides, the limiting current density was about 5.341 mA cm^{-2}, comparable to that of Pt/C.

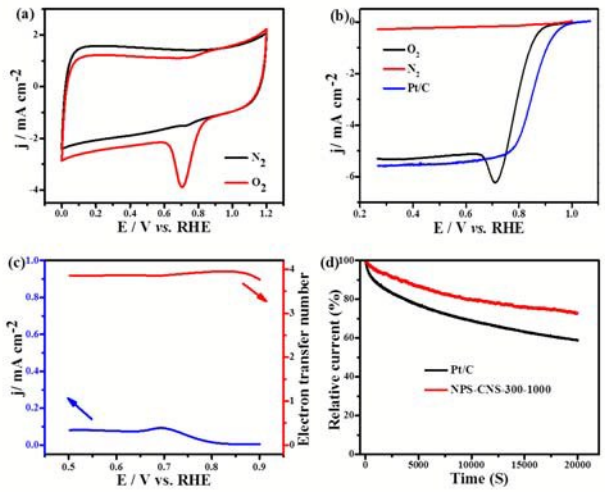

Fig.4 (a) CV curves of NPS-CNS-300-1000 in N_2 and O_2-saturated 0.1 M KOH solution with a scan rate of 50 mV s^{-1}, (b) LSV curves of NPS-CNS-300-1000 and Pt/C in O_2-saturated 0.1 M KOH electrolyte with a scan rate of 10 mV s^{-1}, (c) Current density on ring electrode (blue line) and corresponding electron transfer number (red line) during ORR process. (d) Relative current vs. time of Pt/C and NPS-CNS-300-1000. The metal-free catalyst loading is 0.6 mg cm^{-2}.

ORR can be proceeded in terms of two pathways, i.e. two-electron and four-electron processes. The peroxide species produced by two-electron process are capable of deteriorating the catalysts and membrane, thus leading to the performance degradation of fuel cells.[62,63] Thus four-electron process is prefered. The rotating ring-disk electrode (RRDE) technique was then applied to study the electron transfer process in ORR catalyzed by the studied catalyst. The extremely low current density on ring electrode ranging from 0.9 V to 0.5 V (blue line in Fig. 4c) implied the high selectivity towards four electron pathways during the whole ORR process on NPS-CNS-300-1000. The corresponding electron transfers number (n) was determined to be 3.8~4.0, confirming exclusive four electron transfer process for ORR. In addition, NPS-CNS-300-1000 showed better long-term durability than the commercial Pt/C electrocatalyst (Fig. 4d).

Compared with many previously reported analogous electrocatalysts,[27,64-66] the NPS-CNS-300-1000 is of an outstanding metal-free carbon-based ORR catalyst. The high electrocatalytic activity of NPS-CNS-300-1000 can also be attributed to the unique structure: multi-heteroatom dopants endow high degree of electron redistribution on carbon atoms and create active sites, while high specific surface area and porosity benefit the mass transportation and catalytic sites accessible.

4.Conclusions

In summary, we produced multi-heteroatoms (N, P, S) co-doped ultrathin carbon nanosheets with high specific surface area. Both PZS and g-C_3N_4 nanosheet were key precursors for the final catalysts. PZS coating provided C, N, P, S sources, while g-C_3N_4 nanosheet acted as structural template and extra N doping source as well as porogen to introduce additional mesoporosity of carbon nanosheets. All these features endowed the obtained carbon nanosheets with abundant catalytic active sites and facile diffusion routes. The obtained carbocatalyst exhibited excellent catalytic performance for selective oxidation of aromatic alkanes in aqueous solution and electrochemical oxygen reduction reaction in alkaline medium. The synthetic strategy described in this work is expected to provide a facile and efficient route to prepare multi-heteroatoms co-doped carbon materials as metal-free carbocatalysts with superior catalytic properties.

Acknowledgements

The authors thank the National Natural Science Foundation of China (NSFC 21573245, 21333009, 21273244 and 21573244), and the Chinese Academy of Sciences.

Notes and references

1 K. Yang and B. Xing, *Chem. Rev.,* 2010, **110**, 5989-6008.
2 G. X. Zhao, J. X. Li, X. M. Ren, C. L. Chen and X. K. Wang, *Environ. Sci. Technol.,* 2011, **45**, 10454-10462.
3 H. W. Liang, Q. F. Guan, L. F. Chen, Z. Zhu, W. J. Zhang and S. H. Yu, *Angew. Chem. Int. Ed.,* 2012, **51**, 5101-5105.
4 L. R. Shi, K. Chen, R. Du, A. Bachmatiuk, M. H. Rummeli, K. W. Xie, Y. Y. Huang, Y. F. Zhang and Z. F. Liu, *J. Am. Chem. Soc.,* 2016, **138**, 6360-6363.
5 F. Xu, Z. W. Tang, S. Q. Huang, L. Y. Chen, Y. R. Liang, W. C. Mai, H. Zhong, R. W. Fu and D. C. Wu, *Nat. Commun.,* 2015, **6**, 7221-7230.
6 J. Schuster, G. He, B. Mandlmeier, T. Yim, K. T. Lee, T. Bein and L. F. Nazar, *Angew. Chem. Int. Ed.,* 2012, **51**, 3591-3595.
7 Y.-S. Su and A. Manthiram, *Nat. Commun.,* 2012, **3**, 1166-1171.
8 S. Xin, L. Gu, N.-H. Zhao, Y.-X. Yin, L.-J. Zhou, Y.-G. Guo and L.-J. Wan, *J. Am. Chem. Soc.,* 2012, **134**, 18510-18513.
9 Y.-X. Yin, S. Xin, Y.-G. Guo and L.-J. Wan, *Angew. Chem. Int. Ed.,* 2013, **52**, 13186-13200.
10 Y. W. Zhu, S. Murali, M. D. Stoller, K. J. Ganesh, W. W. Cai, P. J. Ferreira, A. Pirkle, R. M. Wallace, K. A. Cychosz, M. Thommes, D. Su, E. A. Stach and R. S. Ruoff, *Science,* 2011, **332**, 1537-1541.
11 Z.-S. Wu, Y. Sun, Y.-Z. Tan, S. Yang, X. Feng and K. Muellen, *J. Am. Chem. Soc.,* 2012, **134**, 19532-19535.
12 T. Q. Lin, I. W. Chen, F. X. Liu, C. Y. Yang, H. Bi, F. F. Xu and F. Q. Huang, *Science,* 2015, **350**, 1508-1513.
13 J. Liu, N. P. Wickramaratne, S. Z. Qiao and M. Jaroniec, *Nat. Mater.,* 2015, **14**, 763-774.
14 J. Zhang, X. Liu, R. Blume, A. H. Zhang, R. Schlogl and D. S. Su, *Science,* 2008, **322**, 73-77.
15 S. Navalon, A. Dhakshinamoorthy, M. Alvaro and H. Garcia, *Chem. Rev.,* 2014, **114**, 6179-6212.

16 B. Chen, L. Y. Wang and S. Gao, *ACS Catal.,* 2015, **5**, 5851-5876.
17 L. Liu, Y.-P. Zhu, M. Su and Z.-Y. Yuan, *ChemCatChem,* 2015, **7**, 2765-2787.
18 H.-W. Liang, X. Zhuang, S. Bruller, X. Feng and K. Mullen, *Nat. Commun.,* 2014, **5**, 4973-4979.
19 T. Y. Ma, J. R. Ran, S. Dai, M. Jaroniec and S. Z. Qiao, *Angew. Chem. Int. Ed.,* 2015, **54**, 4646-4650.
20 G. Wang, Y. H. Sun, D. B. Li, H. W. Liang, R. H. Dong, X. L. Feng and K. Mullen, *Angew. Chem. Int. Ed.,* 2015, **54**, 15191-15196.
21 J. T. Zhang, L. T. Qu, G. Q. Shi, J. Y. Liu, J. F. Chen and L. M. Dai, *Angew. Chem. Int. Ed.,* 2016, **55**, 2230-2234.
22 M. Zhou, H. L. Wang and S. J. Guo, *Chem. Soc. Rev.,* 2016, **45**, 1273-1307.
23 Y. Zheng, Y. Jiao, M. Jaroniec, Y. Jin and S. Z. Qiao, *Small,* 2012, **8**, 3550-3566.
24 J. Liang, Y. Jiao, M. Jaroniec and S. Z. Qiao, *Angew. Chem. Int. Ed.,* 2012, **51**, 11496-11500.
25 Z. Liu, H. Nie, Z. Yang, J. Zhang, Z. Jin, Y. Lu, Z. Xiao and S. Huang, *Nanoscale,* 2013, **5**, 3283-3288.
26 C. You, S. Liao, H. Li, S. Hou, H. Peng, X. Zeng, F. Liu, R. Zheng, Z. Fu and Y. Li, *Carbon,* 2014, **69**, 294-301.
27 W. Ai, Z. Luo, J. Jiang, J. Zhu, Z. Du, Z. Fan, L. Xie, H. Zhang, W. Huang and T. Yu, *Adv. Mater.,* 2014, **26**, 6186-6192.
28 T. N. Hoheisel, S. Schrettl, R. Szilluweit and H. Frauenrath, *Angew. Chem. Int. Ed.,* 2010, **49**, 6496-6515.
29 S. L. Yang, L. Peng, P. P. Huang, X. S. Wang, Y. B. Sun, C. Y. Cao and W. G. Song, *Angew. Chem. Int. Ed.,* 2016, **55**, 4016-4020.
30 D. Q. Gao, Q. Xu, J. Zhang, Z. L. Yang, M. S. Si, Z. J. Yan, D. S. Xue, *Nanoscale,* 2014, **6**, 2577-2581
31 A. C. Ferrari, J. C. Meyer, V. Scardaci, C. Casiraghi, M. Lazzeri, F. Mauri, S. Piscanec, D. Jiang, K. S. Novoselov, S. Roth and A. K. Geim, *Phys. Rev. Lett.,* 2006, **97**, 187401.
32 I. K. Moon, J. Lee, R. S. Ruoff and H. Lee, *Nat. Commun.,* 2010, **1**, 73-78.
33 Z. H. Li, D. C. Wu, Y. R. Liang, R. W. Fu and K. Matyjaszewski, *J. Am. Chem. Soc.,* 2014, **136**, 4805-4808.
34 H. X. Zhong, J. Wang, Y. W. Zhang, W. L. Xu, W. Xing, D. Xu, Y. F. Zhang and X. B. Zhang, *Angew. Chem. Int. Ed.,* 2014, **53**, 14235-14239.
35 W. H. Niu, L. G. Li, X. J. Liu, N. Wang, J. Liu, W. J. Zhou, Z. H. Tang and S. W. Chen, *J. Am. Chem. Soc.,* 2015, **137**, 5555-5562.
36 J. W. F. To, J. J. He, J. G. Mei, R. Haghpanah, Z. Chen, T. Kurosawa, S. C. Chen, W. G. Bae, L. J. Pan, J. B. H. Tok, J. Wilcox and Z. N. Bao, *J. Am. Chem. Soc.,* 2016, **138**, 1001-1009.
37 Y. J. Gao, G. Hu, J. Zhong, Z. J. Shi, Y. S. Zhu, D. S. Su, J. G. Wang, X. H. Bao and D. Ma, *Angew. Chem. Int. Ed.,* 2013, **52**, 2109-2113.
38 G. Song, F. Wang and X. Li, *Chem. Soc. Rev.,* 2012, **41**, 3651-3678.
39 A. F. M. Noisier and M. A. Brimble, *Chem. Rev.,* 2014, **114**, 8775-8806.
40 C. Liu, J. Yuan, M. Gao, S. Tang, W. Li, R. Shi and A. Lei, *Chem. Rev.,* 2015, **115**, 12138-12204.
41 S. Gaillard, C. S. J. Cazin and S. P. Nolan, *Acc. Chem. Res.,* 2012, **45**, 778-787.
42 X. Wang, D. Leow and J.-Q. Yu, *J. Am. Chem. Soc.,* 2011, **133**, 13864-13867.
43 J. W. Walton and J. M. J. Williams, *Angew. Chem. Int. Ed.,* 2012, **51**, 12166-12168.
44 L. Wang, Y. Zhu, J.-Q. Wang, F. Liu, J. Huang, X. Meng, J.-M. Basset, Y. Han and F.-S. Xiao, *Nat. Commun.,* 2015, **6**, 6957-6964.
45 Y. Wang, H. Li, J. Yao, X. Wang and M. Antonietti, *Chem. Sci.,* 2011, **2**, 446-450.
46 Y. J. Gao, P. Tang, H. Zhou, W. Zhang, H. J. Yang, N. Yan, G. Hu, D. H. Mei, J. G. Wang and D. Ma, *Angew. Chem. Int. Ed.,* 2016, **55**, 3124-3128.
47 X. H. Li and M. Antonietti, *Angew. Chem. Int. Ed.,* 2013, **52**, 4572-4576.
48 C. Zhang, N. Mahmood, H. Yin, F. Liu and Y. Hou, *Adv. Mater.,* 2013, **25**, 4932-4937.
49 Z. Yang, Z. Yao, G. Li, G. Fang, H. Nie, Z. Liu, X. Zhou, X. Chen and S. Huang, *ACS Nano* 2012, **6**, 205-211.
50 Z. -W. Liu, F. Peng, H. -J. Wang, H. Yu, W. -X. Zheng and J. Yang, *Angew. Chem. Int. Ed.,* 2011, **50**, 3257-3261.
51 J. Wang, Z. Xu, Y. Gong, C. Han, H. Li and Y. Wang, *ChemCatChem,* 2014, **4**, 1204-1209.
52 F. Razmjooei, K. P. Singh, M. Y. Song and J.-S. Yu, *Carbon,* 2014, **78**, 257-267.
53 S. Gao, X. Wei, H. Liu, K. Geng, H. Wang, H. Moehwald and D. Shchukin, *J. Mater. Chem. A,* 2015, **3**, 23376-23384.
54 Y. Zhou, R. Ma, S. L. Candelaria, J. Wang, Q. Liu, E. Uchaker, P. Li, Y. Chen and G. Cao, *J. Power Sources,* 2016, **314**, 39-48.
55 M. K. Debe, *Nature,* 2012, **486**, 43-51.
56 J. Wu and H. Yang, *Acc. Chem. Res.,* 2013, **46**, 1848-1857.
57 L. Z. Bu, J. B. Ding, S. J. Guo, X. Zhang, D. Su, X. Zhu, J. L. Yao, J. Guo, G. Lu and X. Q. Huang, *Adv. Mater.,* 2015, **27**, 7204-7212.
58 L. Ma, C. M. Wang, B. Y. Xia, K. K. Mao, J. W. He, X. J. Wu, Y. J. Xiong and X. W. Lou, *Angew. Chem. Int. Ed.,* 2015, **54**, 5666-5671.
59 J. Zhu, S. P. Jiang, R. Wang, K. Shi and P. K. Shen, *J. Mater. Chem. A,* 2014, **2**, 15448-15453.
60 K. Gong, F. Du, Z. Xia, M. Durstock and L. Dai, *Science,* 2009, **323**, 760-764.
61 K. Qu, Y. Zheng, S. Dai and S. Z. Qiao, *Nano Energy,* 2016, **19**, 373-381.
62 R. Zhou, Y. Zheng, M. Jaroniec and S. -Z. Qiao, *ACS Catal.,* 2016, **6**, 4720-4728.
63 Y. Jiao, Y. Zheng, M. Jaroniec and S. Z. Qiao, *J. Am. Chem. Soc.,* 2014, **136**, 4394-4403.
64 J. Liang, Y. Jiao, M. Jaroniec and S. Z. Qiao, *Angew. Chem. Int. Ed.,* 2012, **51**, 11496-11500.
65 J. Liang, Y. Zheng, J. Chen, J. Liu, D. Hulicova-Jurcakova, M. Jaroniec and S. Z. Qiao, *Angew. Chem. Int. Ed.,* 2012, **51**, 3892-3896.
66 G. Wang, Y. Sun, D. Li, H.-W. Liang, R. Dong, X. Feng and K. Müllen, *Angew. Chem. Int. Ed.,* 2015, **54**, 15191-15196.

View Article Online
DOI: 10.1039/C6TA08335H

Journal Name

ARTICLE

Table of Contents (TOC)

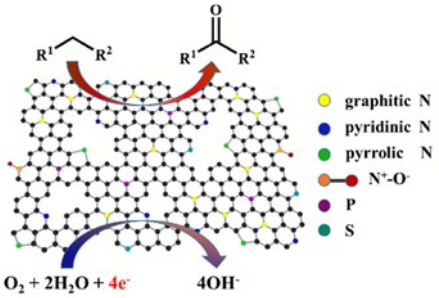

Nitrogen, phosphorus and sulfur co-doped ultrathin carbon nanosheet showed outstanding activity as metal-free catalyst for selective oxidation of aromatic alkanes in aqueous solution and oxygen reduction reaction in alkaline medium.